©Copyright 2016

Jae ook Kim

Microtubule attachment and regulation mechanisms of the budding yeast kinetochore

Jae ook Kim

A thesis

submitted in partial fulfillment of the

requirements for the degree of

Master of Science

University of Washington

2016

Committee:

Trisha N. Davis

Charles L. Asbury

Program Authorized to Offer Degree:

Biochemistry

University of Washington

Abstract

Microtubule attachment and regulation mechanisms of the budding yeast kinetochore

Jae ook Kim

Chair of the Supervisory Committee:

Trisha N. Davis, Professor and Chair

Department of Biochemistry

Strong kinetochore-microtubule attachments are essential for faithful segregation of sister chromatids during mitosis. The Dam1 and Ndc80 complexes are the main microtubule binding components of the budding yeast kinetochore. Cooperation between these two complexes enhances kinetochore-microtubule coupling and is regulated by Aurora B kinase. We show that the Ndc80 complex can simultaneously bind and bridge across two Dam1 complex rings through a tripartite interaction, each component of which is regulated by Aurora B kinase. Mutations in any one of the Ndc80p interaction regions abrogates the Ndc80 complex's ability to bind two Dam1 rings *in vitro,* and results in kinetochore biorientation and microtubule attachment defects *in vivo*. We also show that an extra-long Ndc80 complex, engineered to space the two Dam1 rings further apart, does not support growth. Taken together, our work suggests that each kinetochore *in vivo* might contain two Dam1 rings and that proper ring-ring spacing is vital.

Table of Contents

List of Figures

List of Table

Acknowledgements

I express my gratefulness to Trisha Davis for advising and guiding me through my graduate career not only in science, but also in life as a whole. I grew tremendously from a novice scientist to a capable one that can independently and critically develop hypotheses and experiments. Also, I thank Chip Asbury for the highly collaborative environment, allowing me to carry out biophysical experiments in his lab. His mentoring has led me to develop additional scientific skills that I would not have been able to otherwise. I thank Trisha Davis, Chip Asbury, Rachel Klevit, Jim Hurley, and Justin Kollman for being members of my thesis committee and providing helpful feedback on the thesis. I appreciate present and past members of the Davis lab, especially Neil Umbreit, Alex Zelter, Eric Muller, and Luke Helgeson for working with me and further scientific training. I also thank my family members Chan Kim, Jeol Sook Lee, and Ja-Kyoung Kim for emotional and mental encouragement throughout my graduate career.

Introduction

The kinetochore is a protein supercomplex that assembles on centromeric DNA to physically link the replicated chromosomes to spindle microtubules. Kinetochores harness mechanical force during microtubule depolymerization for segregation of sister chromatids. Understanding how kinetochores maintain strong attachments and how they correct aberrant attachments to microtubules is key for understanding the process of faithful chromosome segregation.

The Dam1 and Ndc80 complexes are the main microtubule-binding components of the budding yeast kinetochore and are individually well characterized. All ten proteins of the Dam1 complex and all four proteins of the Ndc80 complex are essential. Independently, both complexes make diffusive lateral attachments to microtubules, and form load-bearing attachments to microtubule tips (Asbury et al., 2006; Gestaut et al., 2008; Powers et al., 2009; Tien et al., 2010; Umbreit et al., 2014). In addition, the Dam1 complex oligmerizes to form rings on microtubules, which may explain how kinetochores maintain processive attachments to flared microtubules plus-ends. The eukaryotic kinetochore KMN network (KNL1, Mis12, and Ndc80 complexes) interacts with microtubules and is conserved from budding yeast (*S. cerevisiae*) to higher eukaryotes. The yeast-specific Dam1 complex also interacts with microtubules, and may be a functional homolog to the Ska complex in higher eukaryotes (Schmidt et al., 2012; Welburn et al., 2009).

The Dam1 and Ndc80 complexes interact on microtubules to enhance the attachment of Ndc80 complex to microtubules (Lampert et al., 2010; Tien et al., 2010). Despite an abundance of information about each complex, relevant structural and biochemical information about how these two complexes cooperate for strong kinetochore-microtubule attachment is woefully short

and unclear. Through a yeast two-hybrid assay, Maure and coworkers have suggested that the Ndc80p 'loop' region interacts with the Dam1p (Maure et al., 2011). Through microtubule pelleting assays, Lampert and coworkers suggested that the Ndc80p hairpin region interacts with the Dam1 complex (Lampert et al., 2013). In addition, Kalantzaki and coworkers showed an interaction between the Dam1p C-terminal domain and Ndc80p through a yeast two-hybrid assay (Kalantzaki et al., 2015).

In addition to providing strong attachments between chromosomes and spindle microtubules, kinetochores also serve as regulatory hubs. Aberrant kinetochore-microtubule attachments are corrected by Aurora B (Ipl1) kinase to achieve bioriented attachments. In the tension-dependent model, correctly bioriented kinetochores maintain high tension that inhibits Aurora B kinase's activity, whereas incorrectly attached kinetochores lack tension. As a consequence of the lack of tension, Aurora B kinase phosphorylates various kinetochore components to destabilize the non-bioriented attachments, allowing further attempts to make strong, bioriented attachments (Reviewed in Sarangapani & Asbury, 2014). Previous work shows that Aurora B kinase phosphorylates the Dam1 complex in order to disrupt the interaction between the Ndc80 and Dam1 complexes (Cheeseman et al., 2002; Tien et al., 2010); however, specific phosphorylation events required for disrupting the interaction between the two complexes have yet to be deciphered.

In this study, we identify specific interaction sites between the Dam1 and Ndc80 complexes. Each site can be targeted by Aurora B-mediated phosphorylation to disrupt the interaction between the two complexes. We further demonstrate that the Ndc80 complex can simultaneously bind two Dam1 complex rings, forming a bridge of determinate distance. Disrupting the interaction of Ndc80 complex with either one of the two rings results in

kinetochore biorientation defects. Finally, an engineered extra-long Ndc80 complex, which increases the spacing between Dam1 rings, does not support growth *in vivo*. Our results suggest the presence of two Dam1 complex rings per kinetochore *in vivo* and the importance of a specific ring-to-ring distance, defined by an Ndc80 complex bridge.

Results

Three different regions of the Ndc80 complex interact with Dam1p, Ask1p, and Spc34p of the Dam1 complex

We identified where the Dam1 and Ndc80 complexes interact using protein cross-linking and subsequent mass spectrometry analysis (Figure 1A, Supplementary figure 1) following protocols developed previously (Hoopmann et al., 2015; Kudalkar et al., 2015; Tien et al., 2014; Zelter et al., 2015). The C-terminal regions of Dam1p, Ask1p, and Spc34p formed cross-links to three distinct regions of Ndc80p (Figure 1A). These three C-terminal regions of the Dam1 complex include five sites phosphorylated by Aurora B kinase. Phosphorylation of all five sites fully disrupts the interaction between the Dam1 and Ndc80 complexes (Cheeseman et al., 2002; Lampert et al., 2010; Tien et al., 2010). Thus, these sites likely represent the primary interaction sites through which the Dam1 complex binds the Ndc80 complex.

To identify the cognate binding site(s) on Ndc80 complex, we compared the cross-linking data to a map of functional regions on Ndc80p identified from a previous linker-scanning mutagenesis screen (Tien et al., 2013). Three of these functional regions map near or within the regions that cross-link to Dam1p, Ask1p, and Spc34p (Figure 1B). We define these interactions as A, B, and C, and we will refer to the specific regions on each protein that are involved in these interactions as A^{Dam1p} and A^{Ndc80p}, B^{Ask1p} and B^{Ndc80p}, and C^{Spc34p} and C^{Ndc80p}, respectively (Figure 1A; Table 1).

We tested if Ndc80 mutations identified in our screen in regions A^{Ndc80p}, B^{Ndc80p}, and C^{Ndc80p} interfere with interactions between the Ndc80 and Dam1 complexes on microtubules using single-molecule total internal fluorescence (TIRF) microscopy (Figure 1C). Importantly, mutations in regions A^{Ndc80p}, B^{Ndc80p}, or C^{Ndc80p} did not alter the residence time of the Ndc80 complex alone on microtubules, consistent with previous observations (Tien et al., 2013). As reported previously, the presence of the Dam1 complex significantly increases the residence time of wild-type Ndc80 complex on microtubules (Figure 1D) (Tien et al., 2010). However, addition of the Dam1 complex only partially increased the residence time of the mutant complexes as compared to the wild-type Ndc80 complex (Figure 1D; Supplementary figure 2A, B). These observations suggest regions A^{Ndc80p}, B^{Ndc80p}, and C^{Ndc80p} each contribute to the interaction of Ndc80 complex with Dam1 complex.

Dam1p, Ask1p, and Spc34p phosphorylation independently disrupts the interaction between the Dam1 and Ndc80 complexes

We then asked if the corresponding regions in the Dam1 complex also contribute to the interaction between Dam1 and Ndc80 complexes. Aurora B kinase phosphorylates the Dam1 complex at six different sites: Dam1p S20, S257, S265, S292; Ask1p S200; Spc34p T199 (Cheeseman et al., 2002). Phosphorylation of Dam1p S20 significantly decreases the Dam1 complex's apparent affinity for microtubules by inhibiting oligomerization, while phosphorylation of the Dam1p three C-terminal sites slightly decreases the direct affinity of the Dam1 complex for microtubules (Gestaut et al., 2008; Zelter et al., 2015). In our prior work, we mutated Dam1p S20 to alanine, and showed that phosphorylating all five other sites fully disrupts interaction between the Dam1 and Ndc80 complexes (Tien et al., 2010). Here, we determined which combination of these five sites must be phosphorylated to disrupt the

interaction between the Dam1 and Ndc80 complexes. As shown in Figure 1A, we will refer to phosphorylation to the Dam1 complex sites as phosphorylation of regions A^{Dam1p}, B^{Ask1p}, and C^{Spc34p} (Table 1).

Given that the Dam1 complex regions A^{Dam1p}, B^{Ask1p}, and C^{Spc34p} cross-link to Ndc80p, we predicted that phosphorylation of any of these sites would inhibit the interaction between the two complexes. To test this hypothesis, we first purified recombinant mutant Dam1 complexes containing different combinations of Ser/Thr to Ala mutations (together with the S20A mutation in all cases). These mutants were treated with Aurora B kinase to produce a series of Dam1 complexes, each with a unique subset of the sites phosphorylated. Each phosphorylated Dam1 complex was then tested for its ability to bind the wild-type Ndc80 complex in the single-molecule TIRF assay.

Simultaneously phosphorylating all three regions, A^{Dam1p}, B^{Ask1p}, and C^{Spc34p} disrupted the interaction between the Dam1 and Ndc80 complexes completely, as reported previously (Figure 2A; Supplementary figure 2C; Tien et al., 2010). Individually phosphorylating single regions, A^{Dam1p}, B^{Ask1p}, or C^{Spc34p} caused only partial disruption. Phosphorylating region B^{Ask1p} together with C^{Spc34p} also only partially disrupted the interaction, but phosphorylating A^{Dam1p} in combination with either B^{Ask1p} or C^{Spc34p} was sufficient to fully disrupt the interaction (Figure 2B; Supplementary figure 2D, E). Neither the alanine mutations themselves, nor phosphorylation of a mutant Dam1 complex with all six sites mutated to alanine had any effect, confirming that the observed disruptions were due to phosphorylation at these specific sites (Figure 2A; Supplementary figure 2C; Supplementary figure 3). Together these data demonstrate that regions A^{Dam1p}, B^{Ask1p}, and C^{Spc34p} each contribute to the interaction between the Dam1 and Ndc80 complexes and are regulated by phosphorylation.

The Dam1 and Ndc80 complexes interact at three different sites

We next mixed and matched phosphorylation of the Dam1 complex with the mutations in Ndc80p. Full disruption by phosphorylation of the Dam1 complex was recapitulated by substituting a Dam1 complex phosphorylation with its corresponding mutation in Ndc80p. For example, phosphorylation of regions A^{Dam1p} and C^{Scp34p} fully disrupted the interaction between the two complexes (Figure 2B). Similarly, mutation in region A^{Ndc80p} plus phosphorylation at region C^{Scp34p}, or phosphorylation at region A^{Dam1p} plus mutation in region C^{Ndc80p} fully disrupted the interaction between the two complexes (Figure 2C; Supplementary figure G, H).

Phosphorylation combinations that partially disrupted the interaction between the Dam1 and Ndc80 complexes were also recapitulated by substituting a phosphorylation event with mutation in the corresponding binding region of Ndc80p. Phosphorylation at regions B^{Ask1p} and C^{Spc34p} partially disrupted the interaction between the two complexes (Figure 2B). Similarly, mutation in region B^{Ndc80p} plus phosphorylation at region C^{Spc34p}, or phosphorylation at region B^{Ask1p} plus mutation in C^{Ndc80p} partially disrupted the interaction between the two complexes (Figure 2C; Supplementary figure 2F). Together, our results demonstrate that the Dam1 and Ndc80 complexes interact at three different sites, each of which is phospho-regulated by Aurora B kinase.

The Ndc80 complex binds two Dam1 complex rings

The Ndc80 complex is predicted to be a long rod. The coiled-coiled length between regions A^{Ndc80p} and C^{Ndc80p} is predicted to be 29 nm (Lupas & Gruber, 2005) (Figure 3D). The width of a Dam1 complex ring is only ~7 nm across (Ramey et al., 2011). Assuming that the Ndc80 complex adopts a conformation parallel to the microtubule axis (Joglekar et al., 2009), a single ring could not span this distance. We considered that multiple Dam1 complex rings might

bind to the Ndc80 complex. Using negative stain electron microscopy, we imaged the Dam1 complex on microtubules in the absence and presence of the wild-type Ndc80 complex.

The Dam1 complex formed rings on microtubules as previously reported (Miranda et al., 2005; Westermann et al., 2005) (Figure 3A, B). In the absence of the Ndc80 complex, the Dam1 complex rings tended to bind in doublets of rings, at an inter-ring distance of 13.3 ± 2.4 nm (avg ± s.d.) (Figure 3C, Supplementary figure 5A). This suggests that Dam1 complex rings have an affinity for each other along the longitudinal axis of microtubules and have a tendency to stack together. The stacked double-ring organization may be analogous to the paired ring helices previously reported to form at higher concentrations of Dam1 complex (Miranda et al., 2005). In the presence of the Ndc80 complex, doublets of the Dam1 rings were more common. Surprisingly, the two rings in each doublet were consistently held apart by a distance of 33.1 ± 3.8 nm, similar to the predicted coiled-coil length between regions A^{Ndc80p} and C^{Ndc80p} (Figure 3A-C, Supplementary Figure 5B). This suggests that one Ndc80 complex is able to bridge two Dam1 rings by binding one at regions A^{Ndc80p} and B^{Ndc80p} and the second at region C^{Ndc80p}.

To further test this hypothesis, 10 coiled-coil heptad repeats were inserted into Ndc80p and Nuf2p coiled-coil domain between regions B^{Ndc80p} and C^{Ndc80p} (and the corresponding regions in Nuf2p) to increase the length of the coiled-coil domain between the interaction regions by a predicted 10.5 nm (Figure 3D). In the presence of the Ndc80 10-heptad mutant ($Ndc80^{10\text{-}hep}$) complex, Dam1 ring doublets were consistently separated by 42.1 ± 2.1 nm (Figure 3A-C, Supplementary Figure 5C). These results strongly support the hypothesis that the Ndc80 complex bridges two Dam1 rings. Finally, Dam1 rings in the presence of the Ndc80 complexes containing a mutation in region A^{Ndc80p}, B^{Ndc80p}, or C^{Ndc80p} stacked in a manner indistinguishable

from the Dam1 rings alone, in the absence of Ndc80 complex (Supplementary Figure 4, 5D-F). Thus, these mutant Ndc80 complexes are apparently unable to bridge two Dam1 rings.

The Ndc80 10-heptad insertion complex is lethal *in vivo*

The data presented so far raise an interesting hypothesis of the Ndc80 complex binding and bridging two Dam1 complex rings *in vivo*. We then asked if the specific 33.1 nm inter-ring distance, spaced by the Ndc80 complex, is important. To answer this question, we carried out a plasmid shuffle assay and found that *ndc80^{10hep}* could not support growth in the presence of wild-type *NUF2*. We reasoned that having the 10-heptad mutation only on Ndc80p may prevent the Ndc80^{10hep}/Nuf2 dimer from forming. Therefore, we made constructs with the 10-heptad mutation in both Ndc80p and Nuf2p; however, the addition of *nuf2^{10hep}* in the presence of *ndc80^{10hep}* still did not allow growth (Figure 4A).

We did not see a detectable level of Ndc80^{10hep} by immunoblotting (data not shown) and cannot determine if there is a significant amount of ndc80^{10hep} being expressed *in vivo*. Compared to the wild-type Ndc80 complex, the Ndc80^{10hep} complex showed similar microtubule residence times both in the absence and presence of the Dam1 complex (Figure 4B). The Ndc80^{10hep} complex was able to form a complex *in vitro*, as demonstrated by its ability to bind microtubules, interact with Dam1 complex on microtubules, and set inter-Dam1 ring spacing. These results suggest the possibility that the Ndc80^{10hep} complex cannot support viability due to an altered Dam1 complex inter-ring distance.

The Ndc80 mutants exhibit biorientation and attachment defects

The Ndc80p mutants in regions A^{Ndc80p}, B^{Ndc80p}, and C^{Ndc80p} cannot bind two Dam1 complex rings, and consequently have decreased interaction with the Dam1 complex on microtubules. We next asked if the Ndc80p mutants confer defects in chromosome biorientation

and attachment. We used an auxin-inducible degron system for degrading the wild-type Ndc80-AID (Nishimura et al., 2009). Wild-type or mutant *NDC80* was integrated at the *ura3-1* locus. Ndc80-AID was efficiently degraded in the presence of auxin (Supplementary figure 6). Budding index analyses reveal that cells carrying wild-type *NDC80* progressed through mitosis as expected. Cells without *NDC80* also progressed through mitosis despite a significant defect in kinetochore attachment (see below). This suggests that the degradation of Ndc80-AID is sufficient to silence the spindle checkpoint, which is activated through the Ndc80 complex (Dou et al., 2015; Hiruma et al., 2015; Ji et al., 2015). Cells carrying Ndc80p mutations in regions A^{Ndc80p}, B^{Ndc80p}, and C^{Ndc80p} all arrested as large-budded cells (Supplementary figure 7).

For a more detailed analysis of the phenotype conferred by the *NDC80* mutant alleles, we imaged wild-type, depleted, and mutant cells with *CEN3* and spindle pole bodies (SPB) tagged with GFP and mCherry, respectively. In the majority of wild-type *NDC80* cells, two CEN3-GFP puncta were on the spindle axis. At 60 minutes after α-factor release, 78.2% were in metaphase and 21.8 % were in anaphase as judged by the distance between SPBs. In the majority of the Ndc80 depleted cells, CEN3-GFP was off of the spindle axis consistent with complete detachment. Cells with a mutation in region A^{Ndc80p}, B^{Ndc80p}, or C^{Ndc80p} had 61.4, 58.9, and 75.0% of cells with one CEN3-GFP punctum on the spindle axis, and 33.8, 38.9, and 20.8% of cells with one or two CEN3-GFP puncta off spindle axis, respectively. (Figure 5A, B). In addition, in the majority of cells depleted of Ndc80 or with a mutation in regions A^{Ndc80p}, B^{Ndc80p}, or C^{Ndc80p} the SPBs were separated by more than 2 μm (Figure 5C). These observations are consistent with spindle morphology defects reported after disruption of kinetochore-microtubule attachments (Bharadwaj et al., 2004; Cheeseman et al., 2001). Thus, Ndc80 carrying a mutation in region A^{Ndc80p}, B^{Ndc80p}, or C^{Ndc80p} is unable to support normal kinetochore biorientation.

Discussion

The discovery that the Dam1 complex forms oligomers and rings around microtubules galvanized the mitosis field by providing a molecular explanation for how kinetochores are able to maintain processive attachment to the flared ends of a depolymerizing microtubule. Rings are not required for the Dam1 complex to track depolymerizing microtubules in the absence of tension (Gestaut et al., 2008). However, oligomerization of the Dam1 complex is required to maintain attachments under tension as would be experienced during metaphase (Umbreit et al., 2014). Prior models of the kinetochore have all assumed that each kinetochore contains only one Dam1 complex ring. Here we show that the Ndc80 complex binds two rings of the Dam1 complex *in vitro*. Lethal mutations in Ndc80p that block binding of either one of the two rings result in failure of biorientation and attachment *in vivo*. These results suggest that faithful microtubule attachments might require two Dam1 complex rings per kinetochore *in vivo*.

Counting of kinetochore components by fluorescence microscopy has yielded conflicting results for the number of Dam1 complexes at the yeast kinetochore depending on the standard used. Assuming two Cse4 histone molecules per kinetochore, Joglekar and coworkers report enough Dam1 complex sufficient to form one ring at a kinetochore during metaphase and a partial ring during anaphase (Joglekar et al., 2006). Assuming 5.5 Cse4 histone molecules per kinetochore, Lawrimore and coworkers report enough Dam1 complex for two rings at a kinetochore during anaphase (Lawrimore et al., 2011). Our results show that the Ndc80 complex binds two Dam1 rings and are consistent with the latter results.

The hairpin and the loop regions of Ndc80p have both been identified as binding sites for the Dam1 complex (Lampert et al., 2013; Maure et al., 2011). Our results indicate that the interaction between the Ndc80 and Dam1 complexes is more extensive, forming a tripartite

interaction network. The C-terminal domains of Dam1p, Ask1p, and Spc34p interact with three distinct regions of Ndc80p, one of which is the hairpin as previously reported. Our results are also consistent with a previous study showing an interaction between Ndc80p and the C-terminal region of Dam1p (Kalantzaki et al., 2015). However, we did not find any evidence for an interaction between the Ndc80p 'loop' region and Dam1p (Maure et al., 2011).

Aberrant kinetochore-microtubule attachments are phosphorylated and destabilized by Aurora B kinase (Biggins et al., 1999; Cheeseman et al., 2002; Hauf et al., 2003; Pinsky et al., 2006; Tanaka et al., 2002). Aurora B kinase phosphorylation of the Dam1p, Ask1p, and Spc34p C-terminal sites together fully disrupts the interaction between the Dam1 and Ndc80 complexes (Tien et al., 2010). This regulation mechanism has been thought of as binary, either full or non-disruption of the interaction. We show that phosphorylation of certain combinations results in only partial disruption, and full disruption does not require phosphorylation of all three proteins. Our results suggest how the Aurora B kinase might fine tune the interaction between Dam1 and Ndc80 complexes, resulting in a range of disruption.

The inability of *ndc80*^{10hep} and *nuf2*^{10hep} to support growth *in vivo* might be due to the lack of expression of these two genes. If we are able to establish comparable expression of the Ndc80^{10hep} and Nuf2^{10hep}, compared to wild-type Ndc80, we can develop various hypotheses for future work. First, the 33.1 ± 3.8 nm Dam1 complex inter-ring distance, conferred by the wild-type Ndc80 complex, is close to the length of four tubulin dimers within the microtubule lattice. The mutation of 10 heptad repeats in the Ndc80^{10hep} complex results in the addition of 10 nm to the inter-ring distance, or ~1.25 tubulins in length. The Dam1 complex rings might need to be separated by a regular spacing of tubulin dimers for favorable interaction with microtubules. Second, the transition from 13.3 nm to 33.1 nm inter-ring distance, in the absence and presence

of Ndc80 complex, might signal the establishment of kinetochore-microtubule or bioriented attachment, or both. If the 33.1 nm distance signals presence of kinetochore-microtubule attachment, it might also function to silence the spindle assembly checkpoint. Deviation from the 33.1 nm distance might disrupt any of these mitotic checkpoint mechanisms. Future work will focus on determining the expression level of $Ndc80^{10hep}$ and $Nuf2^{10hep}$ and investigating the role of Dam1 ring-ring distance in kinetochore-microtubule attachment and support of growth.

Materials and Methods

Protein expression and purification

The *S. cerevisiae* Ndc80 and Dam1 complexes were independently expressed in *E. coli* using polycistronic vectors, as previously described (Gestaut et al., 2008; Miranda et al., 2005; Powers et al., 2009; Tien et al., 2010; Wei et al., 2005). The Dam1 complex component Spc34p C-terminus was tagged with Hisx6 and the Ndc80 complex component Spc24 N-terminus was tagged with FLAG or Hisx6. Each complex was affinity-purified before further purification through gel filtration. For TIRF microscopy, Nuf2p C-terminus of the Ndc80 complex was tagged with GFP.

Dam1 complex phosphorylation

GST-Ipl1 and GST-Sli15 (residues 554-698) were purified as previously described (Gestaut et al., 2008; Tien et al., 2010; Zelter et al., 2015). GST-Ipl1 (pSB196, Sue Biggins, Fred Hutchinsin Cancer Research Center, Seattle, WA) and GST-Sli15 (residues 554-698) (pSB503, Sue Biggins) were expressed at 23°C and 37˚ C, respectively for 2 hours. GST-Ipl1 was purified using GSTrap HP (GE Healthcare Biosciences) following manufacturer's instructions, except that the elution buffer was 50 mM Tris buffer (pH 8.0), 250 mM KCL, 10 mM glutathione. HiTrap 26/10 Desalting column (GE Healthcare) was used to exchange the buffer to 50 mM HEPES buffer

(pH 7.4), 100 mM NaCl. GST-Sli15 was purified with glutathione-Sepharose 4B resin (GE Healthcare) following manufacturer's instructions, except that the elution buffer was 20 mM Tris buffer (pH 8.0), 200 mM NaCl, 1 mM β-mercaptoethanol, 1 mM EDTA, 10 mM glutathione.

4 μM recombinant Dam1 complex was incubated with 0.5 μM GST-Ipl1, 0.5 μM GST-Sli15, 200 mM NaCl, 10 mM ATP, 25 mM $MgCl_2$, and 50 mM HEPES buffer, pH 7.4. Reaction mixtures were incubated for 90 min at 30°C. Under these conditions, we achieve nearly stoichiometric phosphorylation of the complex (Gestaut et al., 2008). Mock treated (non-phosphorylated) controls of the Dam1 complex was carried out by substituting ATP with dH_2O.

TIRF microscopy

Glass slides and functionalized coverslips were used to construct flow chambers, as reported previously (Gestaut et al., 2008; Gestaut et al., 2010; Tien et al., 2010; Zelter et al., 2015). A coverslip was adhered to a glass slide with double-sided tape, forming a flow chamber between two adjacent strips of tape. 'Rigor' kinesin was flowed through the chamber to unspecifically bind to the coverslip. Taxol-stabilized, Alexa-647-labelled microtubules were then flowed in and incubated for 5 minutes for immobilization. For all TIRF microscopy experiments, Ndc80-GFP complex was incubated at 50 pM for single-molecule imaging. Each phosphorylated or mock-treated Dam1 complex mutant construct was incubated at 2.5 nM. GFP and Alexa-647 fluorescence channels were simultaneously recorded using a custom TIRF imaging system (Gestaut et al., 2010). All TIRF microscopy experiments were carried out in BRB80 (80 mM PIPES buffer (pH. 6.8), 1 mM EGTA, 1 mM $MgCl_2$) in the presence of 8 mg/ml BSA, 0.04 mg/ml κ-casein, and an oxygen scavenger system (200 μg/ml glucose oxidase, 35 μg/ml catalase, 25 mM glucose, and 5 mM DTT).

Analysis of the single particle tracking was carried out as previously described (Tien et al., 2010; Umbret et al., 2014; Zelter et al., 2015). Custom analysis software (available upon request) was developed in Labview (National Instruments) and Igor Pro (Wavemetrics). Bootstrapping analysis was used to calculate the mean residence times (Umbreit et al., 2014). Randomly resampling each dataset with replacement was repeated 1,000 times. Carrying out this method with each dataset yielded normal distributions. Gaussian fits to these distributions were used to estimate the mean residence times and the width of the fit was used as an estimate of error.

Chemical Cross-linking and Mass Spectrometry Analysis (XL-MS)

XL-MS was performed as described in Zelter et al. 2015. Briefly, 10 µg of taxol stabilized microtubules were mixed with 10 µg Dam1 complex and 10 ug Ndc80 complex in 100 µL BRB80 at 25^{o}C and allowed to stand for 5 mins. For DSS cross-linking, 3 µL 14.5 mM DSS in DMSO was added, and the mixture allowed to cross-link for 2 mins at 25^{o}C before quenching by addition of 10 µL 0.5 M NH_4HCO_3. For EDC cross-linking 7.5 µL 145 mM EDC plus 3.75 µL 145 mM Sulfo-NHS were added to the reaction, and the mixture allowed to cross-link for 30 mins at 25^{o}C before quenching by addition of 10 µL 0.5 M NH_4HCO_3. Quenched reactions were spun at 58,000 rpm in a TLA100 rotor for 10 minutes at 37^{o}C. The pellet was resuspended in 100 µL ice cold buffer reduced with 10 mM dithiothreitol (DTT) at 37^{o}C for 30 mins followed by 30 mins alkylation at RT with 15 mM iodoacetamide (IAA). Digestion with trypsin at a substrate to enzyme ratio of 60:1 was performed overnight at room temperature with shaking. Digested samples were acidified with 5M HCL prior to being stored at -80°C until analysis. Mass spectrometry and data analysis was performed on either a Q-Exactive or Q-Exactive HF (Thermo Fisher Scientific) as previously described (Zelter et al., 2015). Mass spectra were converted into

mzML using msconvert from ProteoWizard (Chambers et al., 2012). Standard linear peptide searches were performed using Comet (Eng et al., 2013). Cross-linked peptides were identified using the Kojak version 1.4.2 cross-link identification software (Hoopmann et al., 2015) following the author's instructions (http://www.kojak-ms.org). Kojak results were exported to Percolator (Käll et al., 2007) to produce a statistically validated set of cross-linked peptide identifications at the desired false discovery rate (FDR) threshold. All the data presented in the current work including raw MS spectra and search parameters used, are available at: http://proxl.yeastrc.org/proxl/viewProject.do?project_id=24.

Electron Microscopy

Cleared tubulin was polymerized in a total volume of 40 µl BRB80 (80 mM PIPES buffer (pH 6.8), 1 mM EGTA, 1 mM $MgCl_2$) containing 1.75 mM GTP, 1 mM $MgCl_2$, and 3.5% DMSO at 37°C for 30 min. Microtubules were pelleted and resuspended in BRB80 containing 10 µM taxol. All samples were prepared in BRB80 + 10 µM taxol by mixing 20 nM microtubules, and 25 nM Dam1 in the absence or presence of 25 nM Ndc80 complex. Samples were incubated at room temperature for 15 minutes. Carbon-coated copper grids were negatively discharged in a glow discharge device. A 5 µl volume of sample was applied on a discharged grid for 20 s before being blotted. 6 µl 2% uranyl acetate was then applied on the grid and incubated for 1 min. The grid was blotted and air dried. EM samples were viewed on a transmission electron microscope (Morgagni; FEI) operating at 100 kV. Images were recorded on a bottom-mounted Orius (Gatan) camera at 22,000x magnification. ImageJ was used to measure the Dam1 complex inter-ring distances. Distances from middle of a ring to the middle of the next closest ring, on both sides, were measured.

Test for function of Ndc80^{10hep} complex

Strains used in this study are derivatives of SBY3 (W303; supplementary table 1). To test if the Ndc80^{10hep} complex is functional *in vivo*, we used a red/white plasmid shuffle assay (Davis, 1992; E. G. Muller, 1996) using strain JTY5-8B (*ade2-1oc ade3Δ-100 leu2-3,112 ura3-1 ndc80Δ::NatMX*), transformed with pJT12 (*NDC80 ADE3* in a 2-μm vector). JTY5-8B was transformed with pJOK13 (*URA3 ndc80^{10hep}*) and selected for growth on SD-ura low adenine plates. Transformation with pJOK13 yielded non-sectoring red colonies (strain JOKY3) demonstrating that the *ndc80^{10hep}* is not viable when paired with wild-type *NUF2* (data now shown). JOKY3 was then transformed with pJOK018 (*LEU2 nuf2^{10hep}*), pJOK019 (*LEU2 NDC80*), or pRS315 (*LEU2*) and plated on SD-ura-leu plates. Several colonies from each transformation were streaked onto SD-ura low-ade plates to screen for sectoring colonies.

Yeast live-cell imaging and analysis

Strains for live-cell imaging were constructed using previously described strains: *SPC110-mCherry, pCUP1-GFP-LacI12* and *CEN3::33LacO* (Wargacki et al., 2010); *NDC80-3V5-IAA7* and *pGPD1-TIR1* (Miller et al., 2016). Sue Biggins kindly provided the Ndc80-AID strain. Strains containing *NDC80*, *ndc80-314* (ins A^{Ndc80p}), *ndc80-383* (ins B^{Ndc80p}), or *ndc80-563* (ins C^{Ndc80p}) were constructed through an integration method previously described (Widlund & Davis, 2005).

Asynchronously growing cells (30 Klett) were subjected to YPD + 6 μM α-factor arrest for 2 hours. Auxin (IAA) was then introduced to incubate the cells in YPD + 6 μM α-factor + 0.5 mM IAA medium for 1 hour. The cells were released from α-factor into YPD + 0.5 mM IAA medium

and imaged at 15 minute time-intervals from time 0 to 120 min. At each time point, cells were also fixed in formaldehyde for budding index analysis. For all the strains tested, 60 min time point was chosen for data collection. Cells were placed on agar pads prior to imaging, as previously described (Muller et al., 2005). Cells were imaged using a DeltaVision system (Applied Precision) equipped with IX70 inverted microscope (Olympus), a Coolsnap HQ digital camera (Photometrics), and an U Plan Apo 100X objective (1.35 NA). *CEN3-LacI* was visualized with the presence of *GFP-LacO* and *SPC110-mCherry* was visualized for tracking the spindle pole bodies. Both GFP and mCherry were imaged with 0.4 s exposures with 16, 0.2 μm z-sections. Images were binned 2 x 2 with a final resolution of 512 x 512. Biorientation analysis was done manually for those cells with 2 mCherry puncta through Imaris software (Bitplane).

Western blot analysis

During the yeast live-cell imaging, samples were collected for western blot analysis. After the addition of auxin, cell samples were collected at various time points. 0.7 ml cells and 0.7 ml 20% tricholoroacetic acid were incubated at 4°C for 1 hour. Sample was pelleted for at 20,000xg for 10 min at 4°C. Pellet was washed by resuspending in 1 ml 4°C ethanol. Sample was then pelleted and resuspended once more before a final pelleting step. Supernatant was discarded and sample was air dried before resuspending in 50 μl 0.1N NaOH, SDS-PAGE sample buffer. Western blot experiments were carried out, probing for Ndc80p (gift from Arshad Desai, Ludwig Cancer Research Center, University of California San Diego) and β-Actin (Abcam). Protein levels analysis was carried out using Image Studio Lite (Li-Cor).

Figures

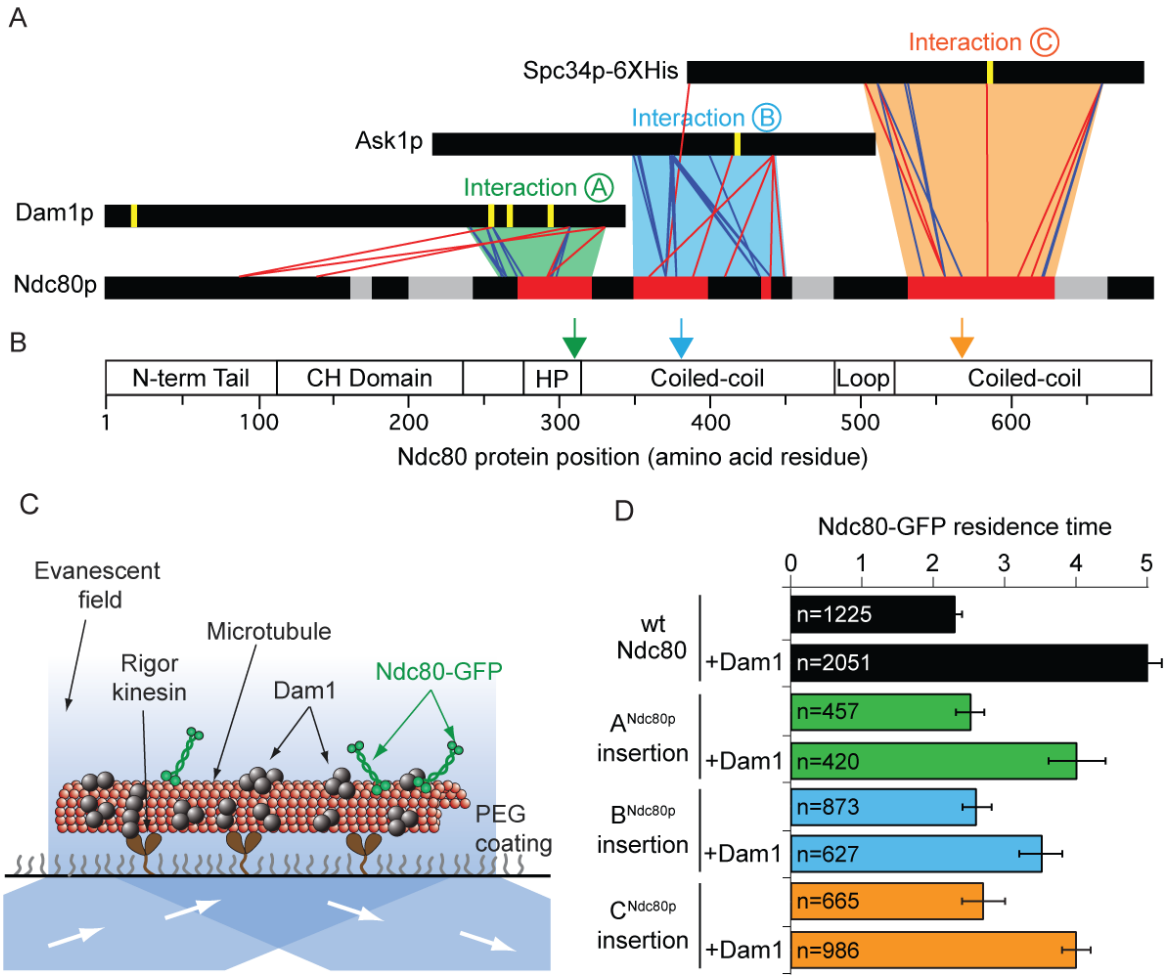

Figure 1

Dam1p, Ask1p, and Spc34p form cross-links to three distinct regions in Ndc80p.

(A) Cross-links between the Dam1p, Ask1p, and Spc34p of the Dam1 complex and Ndc80p of the Ndc80 complex. Dam1 and Ndc80 complexes were cross-linked in the presence of microtubules. Horizontal black bars represent proteins and the six vertical yellow lines indicate Aurora B kinase phosphorylation sites on the Dam1 complex. Red and blue lines show cross-links formed with DSS and EDC cross-linkers, respectively. For clarity, only the cross-links between the Dam1 complex proteins and Ndc80p are displayed. Red bars on Ndc80p indicate regions where clusters of lethal mutations mapped (from Tien et al., 2013) and cross-links occurred. Grey bars on Ndc80p indicate clusters of lethal insertions outside of cross-linked regions. Green, blue, and orange trapezoids represent putative interaction sites between the Dam1 and Ndc80 complexes. (B) Bar diagram of Ndc80p with structural features. Green, blue and orange arrows indicate the positions of lethal mutations in interaction regions A^{Ndc80p}, B^{Ndc80p}, and C^{Ndc80p} used in this study. (CH: calponin homology; HP: hairpin) (C) Diagram showing the setup of TIRF microscopy experiments. Single molecule Ndc80-GFP complex binding on microtubules was visualized in the presence or absence of the Dam1 complex. (D) Average residence time of Ndc80-GFP mutant and wild-type complexes on microtubules in the presence or absence of Dam1 complex. Bars represent average residence time ± error of the mean (estimated by bootstrapping analysis; see Methods for additional details).

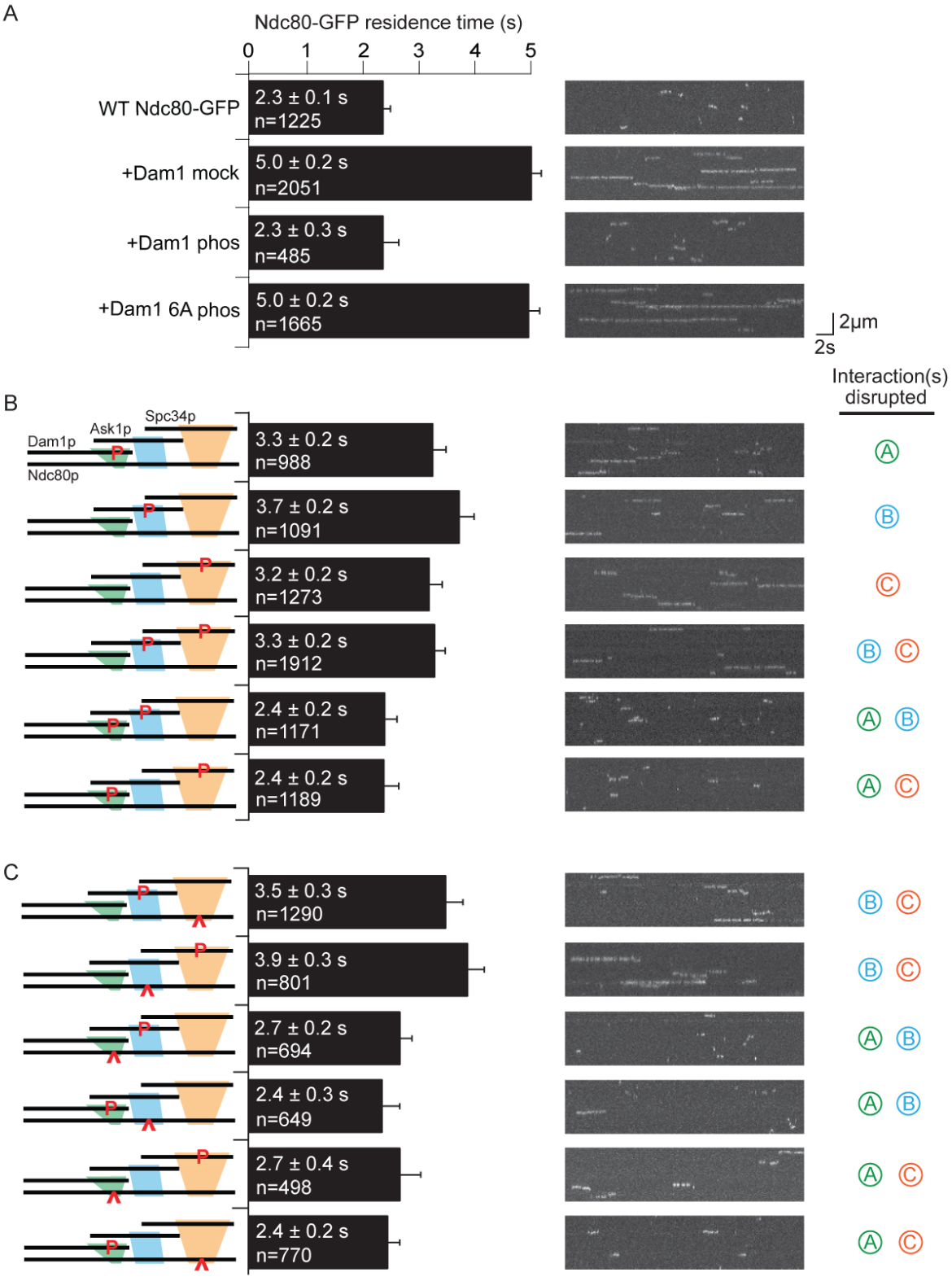
A
Ndc80-GFP residence time (s)
0
1
2
3
4
5
WT Ndc80-GFP
2.3 ± 0.1 s
n=1225
+Dam1 mock
5.0 ± 0.2 s
n=2051
+Dam1 phos
2.3 ± 0.3 s
n=485
+Dam1 6A phos
5.0 ± 0.2 s
n=1665
2μm
2s
Interaction(s) disrupted
B
Dam1p
Ask1p
Spc34p
Ndc80p
P
3.3 ± 0.2 s
n=988
3.7 ± 0.2 s
n=1091
3.2 ± 0.2 s
n=1273
3.3 ± 0.2 s
n=1912
2.4 ± 0.2 s
n=1171
2.4 ± 0.2 s
n=1189
A
B
C
C
3.5 ± 0.3 s
n=1290
3.9 ± 0.3 s
n=801
2.7 ± 0.2 s
n=694
2.4 ± 0.3 s
n=649
2.7 ± 0.4 s
n=498
2.4 ± 0.2 s
n=770

Figure 2
Dam1 and Ndc80 complexes have a tripartite interaction on microtubules.
(A) Average microtubule residence time of the wild type Ndc80-GFP complex alone, in the presence of mock treated, phosphorylated Dam1 complex, or phosphorylated Dam1 6A mutant complex. Dam1 6A: all six Dam1 complex phosphorylation sites mutated to Ala. (B) Average microtubule residence time of wild type Ndc80-GFP complex in the presence of selectively phosphorylated Dam1 complex. Diagram on the left indicates phosphorylated proteins. (C) Average microtubule residence time of Ndc80-GFP complex with lethal mutation in region A^{Ndc80p}, B^{Ndc80p}, or C^{Ndc80p} in the presence of selectively phosphorylated Dam1 complex. Diagrams on the left indicate phosphorylated protein (P) and Ndc80p region with a lethal mutation (^). On the right are representative kymographs for each experiment. Bars represent average residence time ± error of the mean (estimated by bootstrapping analysis; see Methods or additional details).

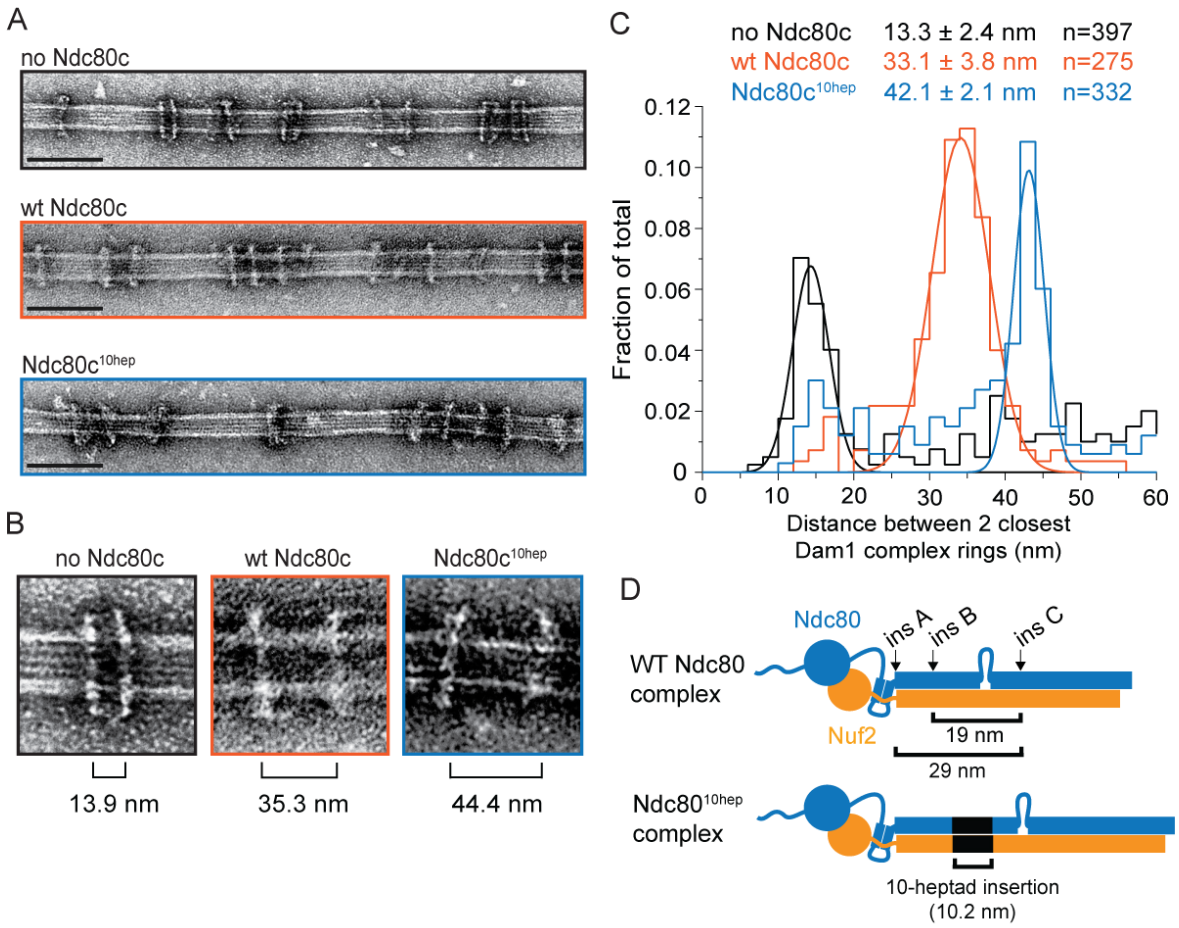

Figure 3
The Ndc80 complex binds two Dam1 complex rings.
(A) Representative EM images of Dam1 complex rings on microtubules in the absence or presence of the Ndc80 complex (Ndc80c). Three experiments include no Ndc80 complex, wild type Ndc80c, and Ndc80c^{10hep}. Protein concentrations were 20 nM tubulin and 25 nM Dam1 and Ndc80 complexes. Scale bars: 100 nm. (B) Zoomed in images of a Dam1 complex ring doublet for the three experiments. Distances from middle of one ring to that of the next ring are indicated. (C) Distribution of closest inter-ring distances measured for the three different experiments. Measurements made between 0-60 nm are shown. The cluster of distance measurements was fitted with a Gaussian distribution and the vertices ± standard deviations for each fit are listed. (D) Diagram demonstrating the predicted coiled-coil distances between the Ndc80p lethal mutations. Diagram below shows the location of additional 10-heptad insertion between the hypothesized binding sites of two Dam1 complex rings.

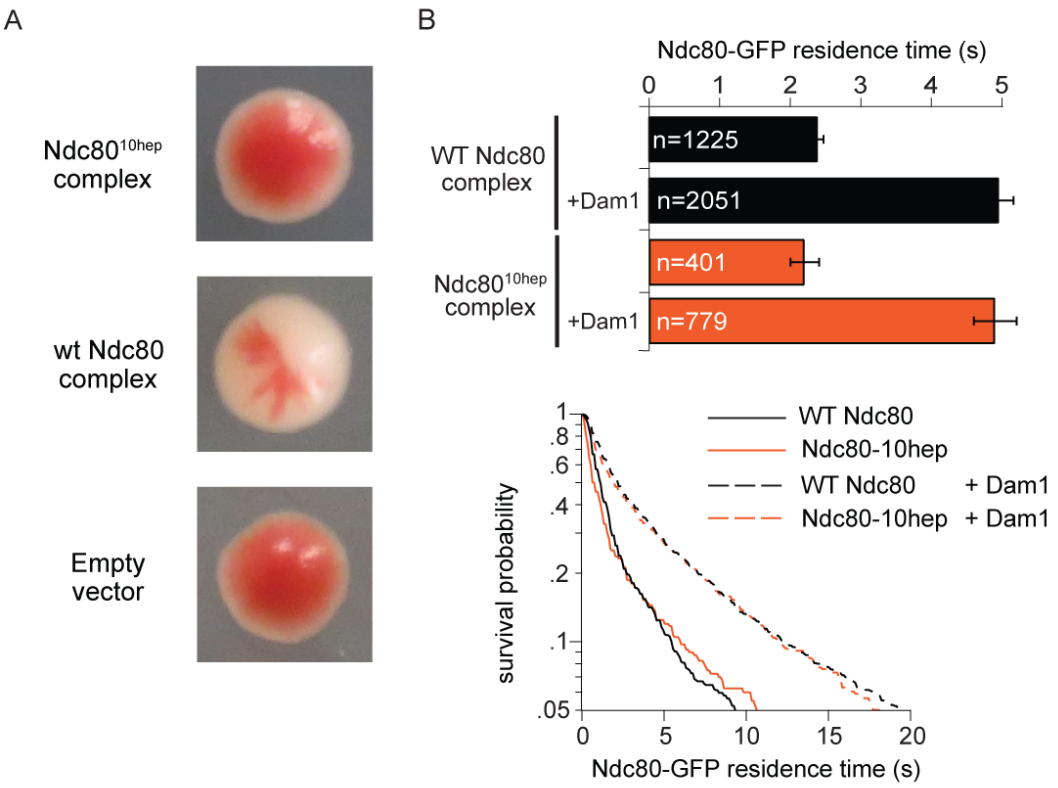

Figure 4
The Ndc80^{10hep} complex does not support growth.
(A) Red/white plasmid shuffle assay for testing the viability of the Ndc80^{10hep} complex. Solid red colonies indicate the inability of the Ndc80^{10hep} complex and empty vector to support growth. Sectoring white colony indicates the ability of the wild type Ndc80 complex to support growth.
(B) Wild-type or Ndc80^{10hep} complex average residence time on microtubules in the absence and presence of Dam1 complex as derived from the survival probability curves (below).

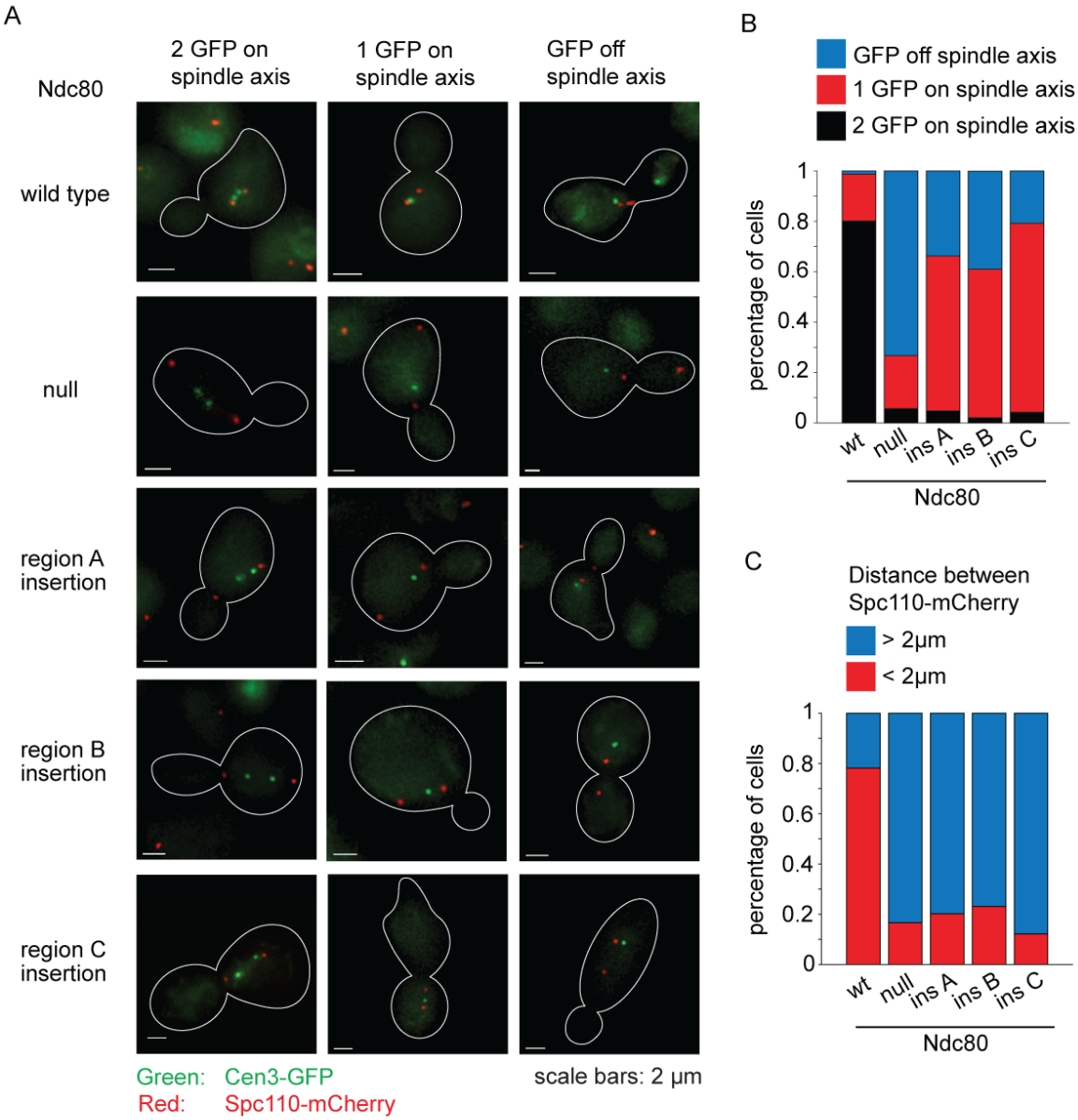

Figure 5

Lethal mutations in A^{Ndc80p}, B^{Ndc80p}, and C^{Ndc80p} have biorientation and microtubule attachment defects *in vivo*.

(A) Representative images from Ndc80-AID degron experiments with cells carrying an extra copy of *NDC80* wild type, no *NDC80*, mutations (mut) in A^{Ndc80p}, B^{Ndc80p}, or C^{Ndc80p}. Cells were treated with 6 µM α-factor for two hours prior to treatment with 6 µM α-factor and 0.5 mM auxin for one additional hour. At time 0, cells were released from α-factor and incubated in YPD medium containing 0.5 mM auxin. Images were taken at 60 min. (B) Stacked bar graphs showing proportion of the cells containing one or two CEN3-GFP puncta off the spindle axis, one CEN3-GFP punctum on the spindle axis, or two CEN3-GFP puncta on the spindle axis. Only cells with two SPB-mCherry puncta and at least one CEN3-GFP punctum were included in the analysis. (C) Stacked bar graph showing the distance between SPB-mCherry puncta.

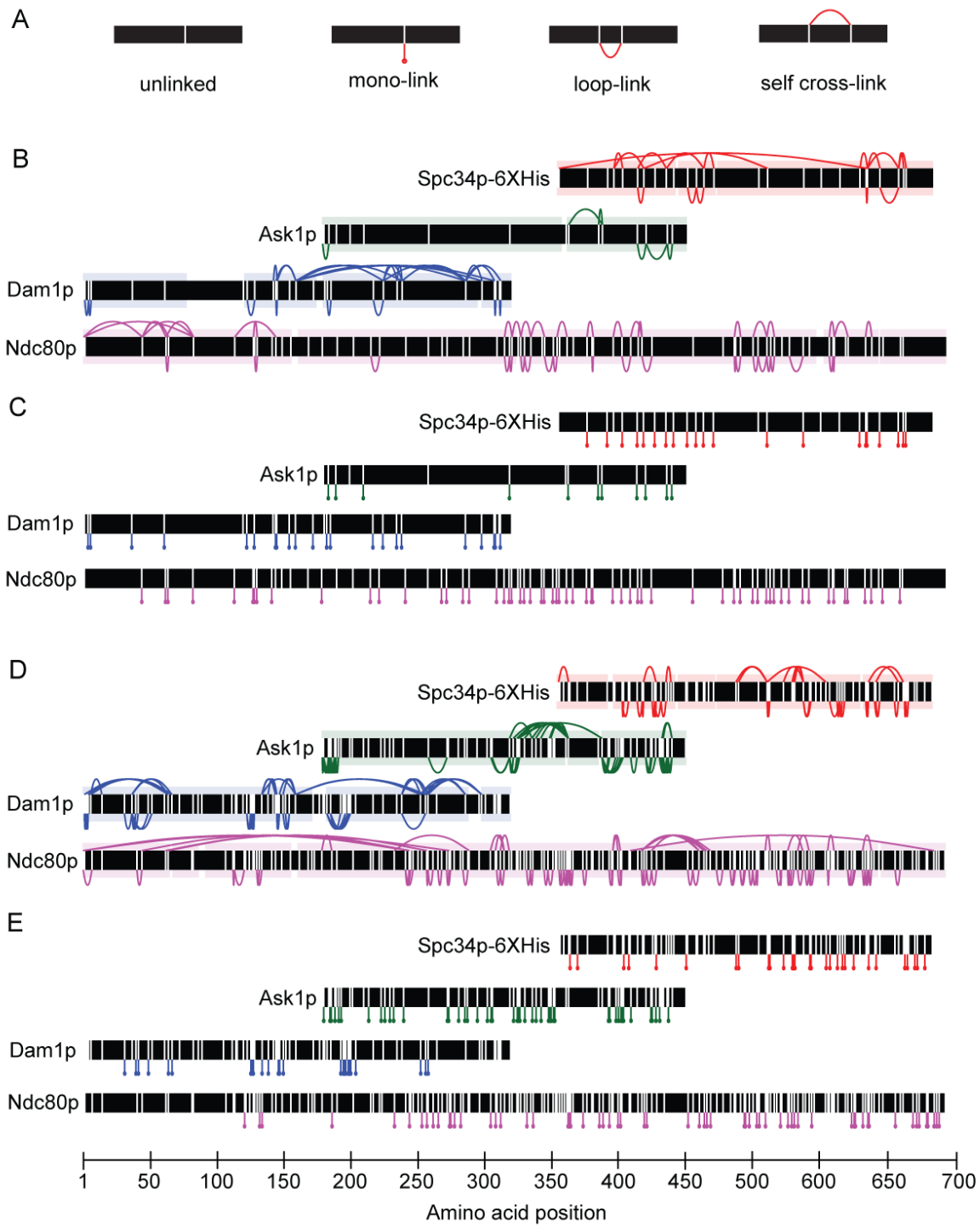
A
unlinked
mono-link
loop-link
self cross-link
B
Spc34p-6XHis
Ask1p
Dam1p
Ndc80p
C
Spc34p-6XHis
Ask1p
Dam1p
Ndc80p
D
Spc34p-6XHis
Ask1p
Dam1p
Ndc80p
E
Spc34p-6XHis
Ask1p
Dam1p
Ndc80p
1
50
100
150
200
250
300
350
400
450
500
600
650
700
Amino acid position

Supplementary Figure 1
Dam1 and Ndc80 complexes robustly react with DSS and EDC cross-linking agents.
(A) Four types of peptides identified by mass spectrometry after cross-linking and trypsin digestion. Horizontal black bars represent protein sequence and vertical white lines represent residues able to react with the cross-linking agent. Unlinked: peptide that did not react with cross-linking agent; mono-link: only one end of the cross-linking reagent reacted with a residue; loop-link: intra-protein cross-link without a tryptic site in between the two cross-linked residues; self cross-link: intra-protein cross-link with a tryptic site in between the two-cross-linked residues. Dam1 and Ndc80 complexes were cross-linked in the presence of microtubules using DSS (B), (C) or EDC (D), (E) cross-linker. (B, D) Cross-links above and below black bars represent self-crosslinks and loop-links, respectively. Highlighted regions above and below black bars represent sequence coverage from mass spectrometry. (C, E) Lines below black bars represent mono-links.

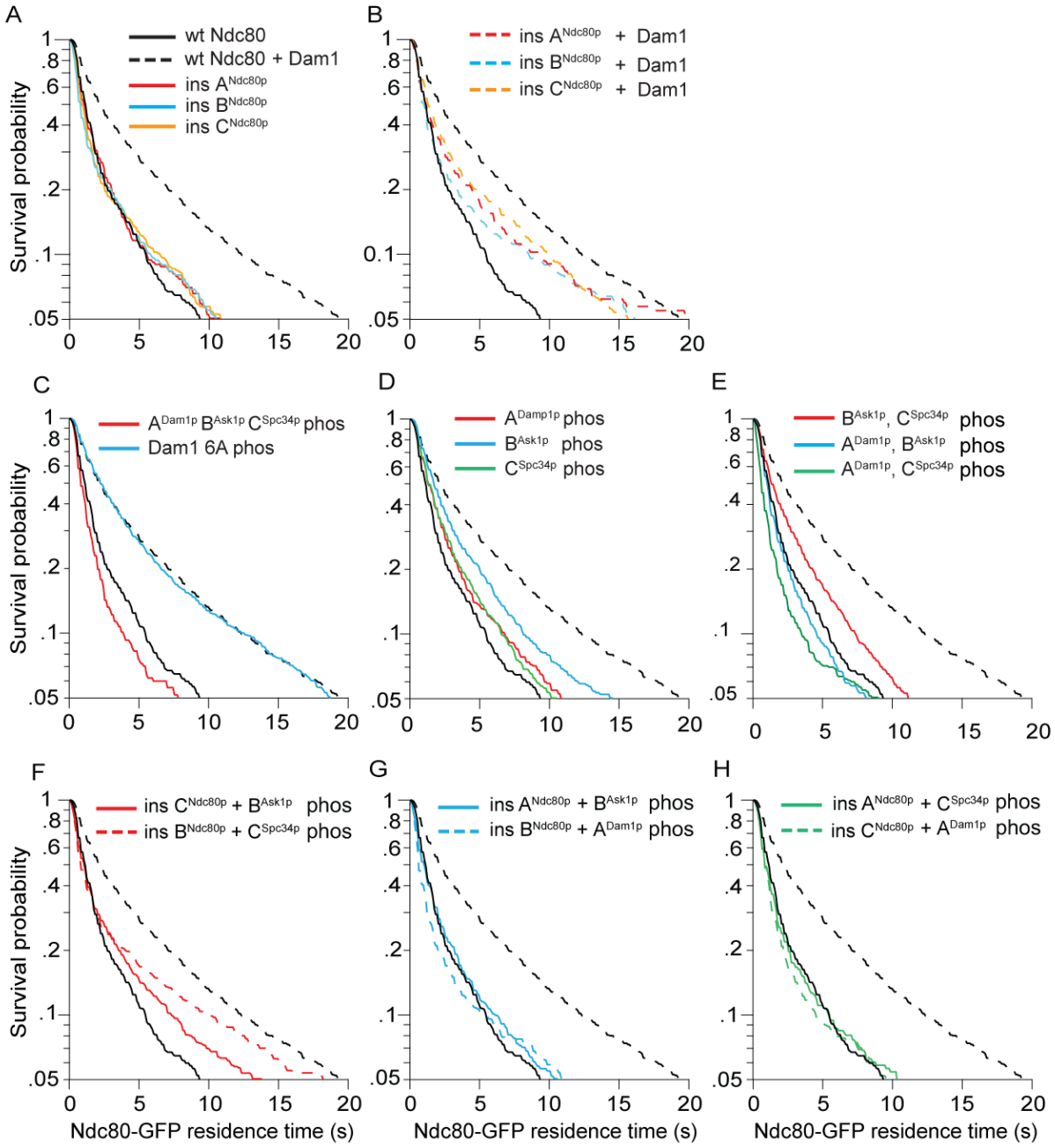

Supplementary Figure 2
Survival probability plots of various Ndc80-GFP complex residence time on microtubules. For all graphs, solid and dashed black lines represent curves for wild-type Ndc80 complex in the absence and presence of wild-type Dam1 complex, respectively. (A), (B) Microtubule residence time of Ndc80-GFP complex with a lethal mutation in region A^{Ndc80p}, B^{Ndc80p}, or C^{Ndc80p} in the absence (A) and presence (B) of wild-type Dam1 complex. (C)-(E) Wild-type Ndc80-GFP complex microtubule residence time in the presence of variably phosphorylated Dam1 complex. Dam1 6A phos: all Dam1 complex phosphorylation sites mutated to Ala and treated with Aurora B kinase. (F)-(H) Microtubule residence time of Ndc80-GFP complex with a mutation in region A^{Ndc80p}, B^{Ndc80p}, or C^{Ndc80p} in the presence of variably phosphorylated Dam1 complex.

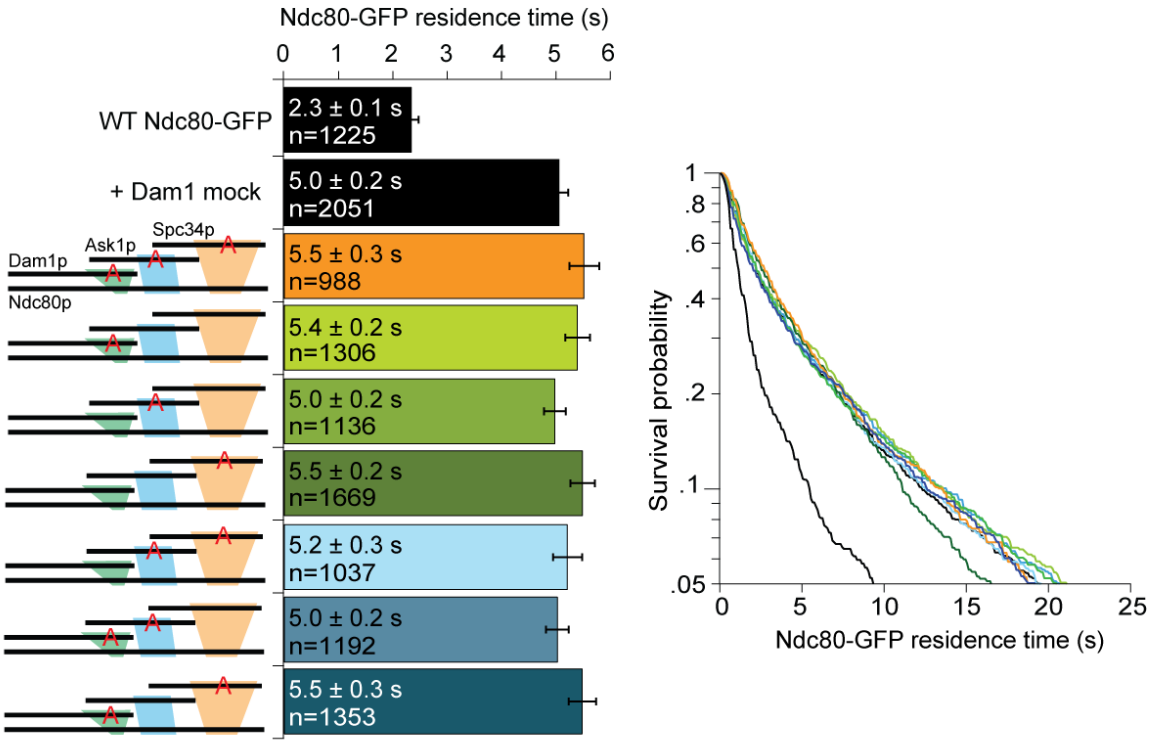

Supplementary Figure 3
Mutating Dam1 complex Aurora B kinase phosphorylation sites to Ala does not affect the interaction between Dam1 and Ndc80 complexes.
(A) Average microtubule residence time of wild-type Ndc80-GFP complex in the presence of various mock treated phosphorylation-blocking Dam1 complex mutant constructs. Mock treatment was carried out by substituting ATP with H_20. (B) Survival probability plots of the experiments displayed in (A).

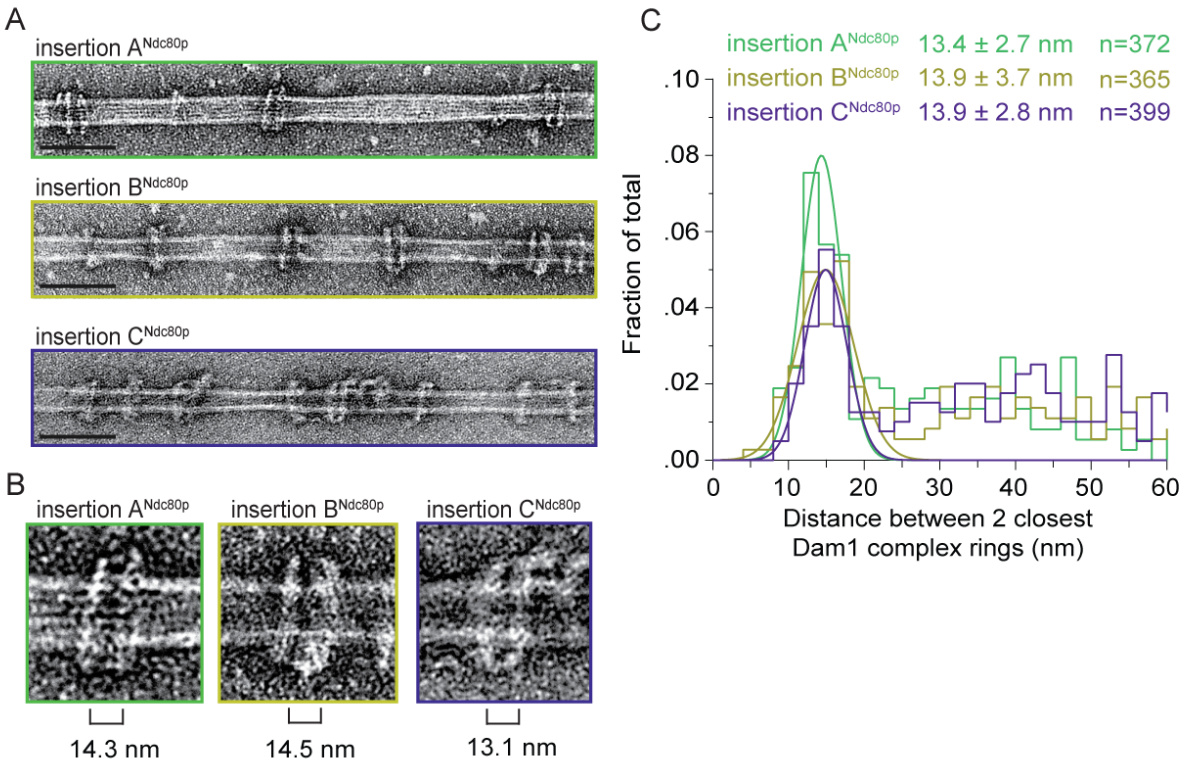

Supplementary Figure 4
Mutations in regions A^{Ndc80p}, B^{Ndc80p}, or C^{Ndc80p} disrupts the Ndc80 complex's ability to bind two Dam1 complex rings.
(A) Representative EM images of Dam1 complex rings on microtubules in the presence of the Ndc80 complex with a mutation in region A^{Ndc80p}, B^{Ndc80p}, or C^{Ndc80p}. Scale bars: 100 nm. Protein concentrations were 20 nM tubulin and 25 nM Dam1 and Ndc80 complexes. (B) Zoomed in images of a Dam1 complex ring doublet for the three experiments. Distances from middle of one ring to those of the closest two rings were measured. (C) Distribution of closest inter-ring distances measured for the three experiments. Measurements made between 0-60 nm are shown. The cluster of distance measurements was fitted with a Gaussian distribution and the vertex ± standard deviation for each fit is listed.

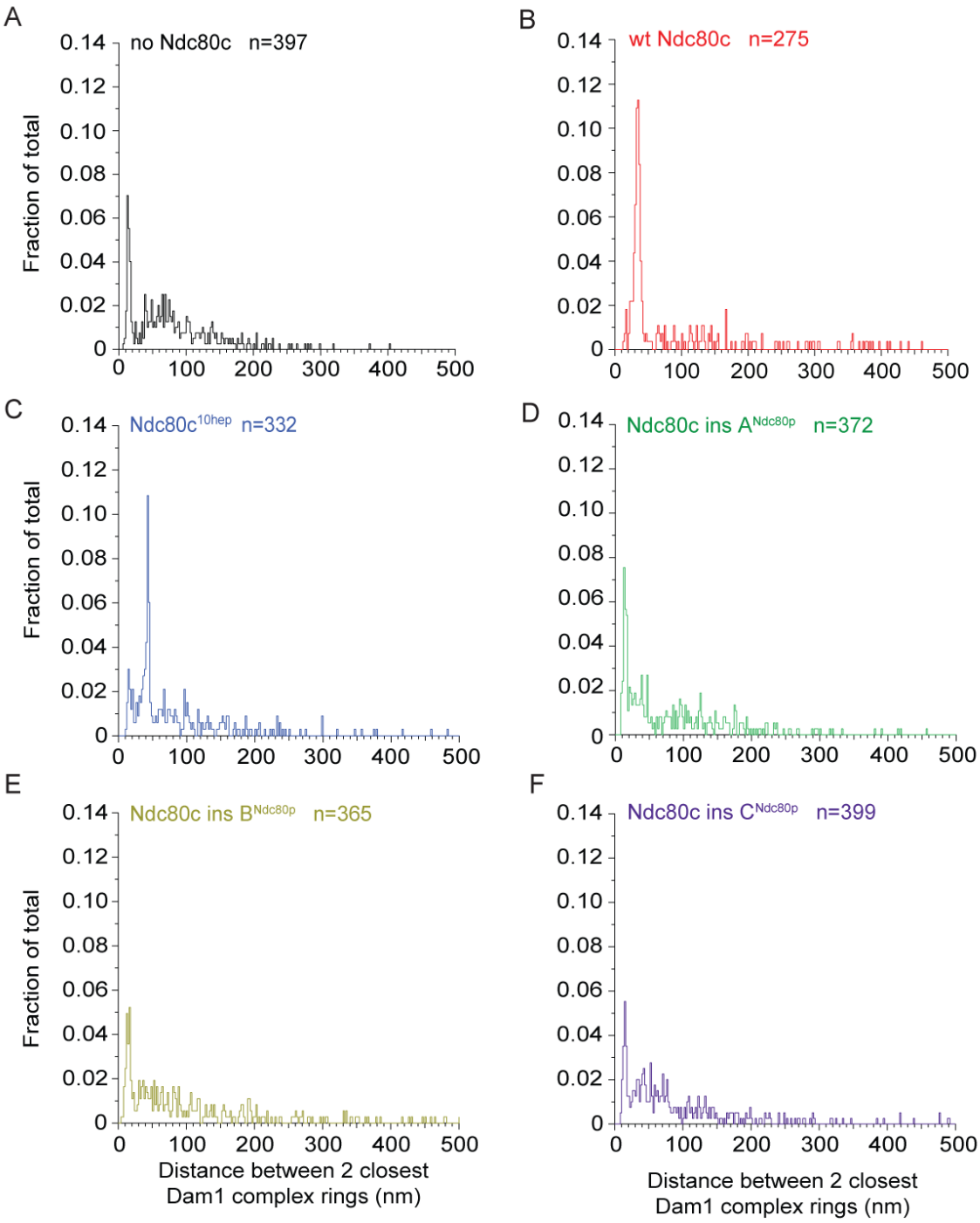

Supplementary Figure 5
Full distributions of Dam1 complex inter-ring measurements for various experiments shown in Figure 3 and Supplementary figure 4. Six conditions include Dam1 complex rings on microtubules in the absence of Ndc80 complex (Ndc80c) (A), presence of wild type Ndc80c (B), Ndc80c^{10hep} (C), Ndc80c mutation A^{Ndc80p} (D), Ndc80c mutation B^{Ndc80p} (E), and Ndc80c mutation C^{Ndc80p} (F).

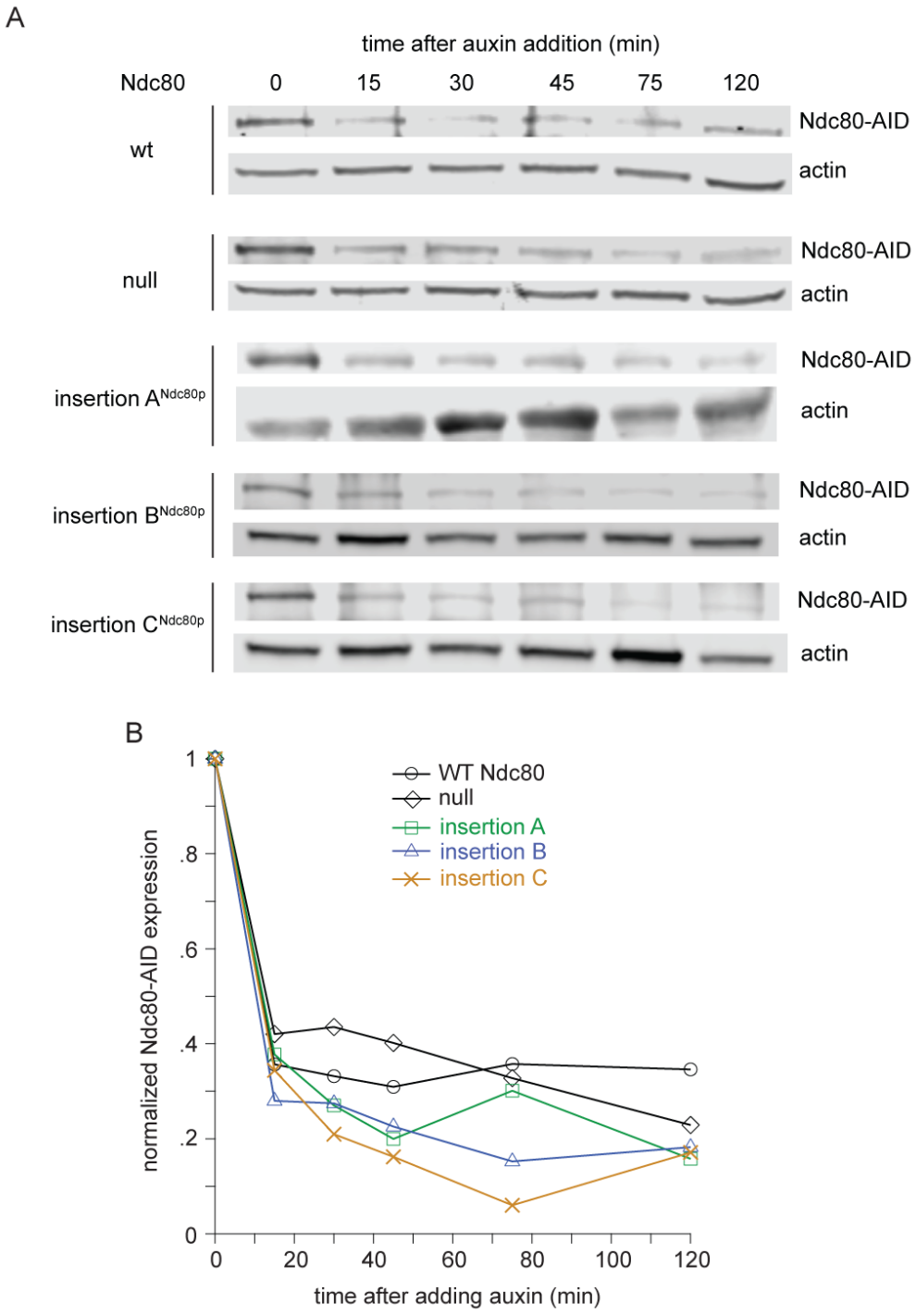

Supplementary Figure 6
Wild-type Ndc80-AID is degraded upon the addition of auxin.
(A) Western blot images from Ndc80-AID degron experiments, blotting for Ndc80-AID and β-actin. Whole cell protein precipitation was carried out for Ndc80-AID cells carrying an extra copy of *NDC80* wild type, no *NDC80* (null), mutation in A^{Ndc80p}, B^{Ndc80p}, or C^{Ndc80p}. Samples were collected at various time points after adding auxin (images were taken 120 min after auxin addition). (B) Normalized Ndc80-AID protein levels analyzed by western blot band intensities.

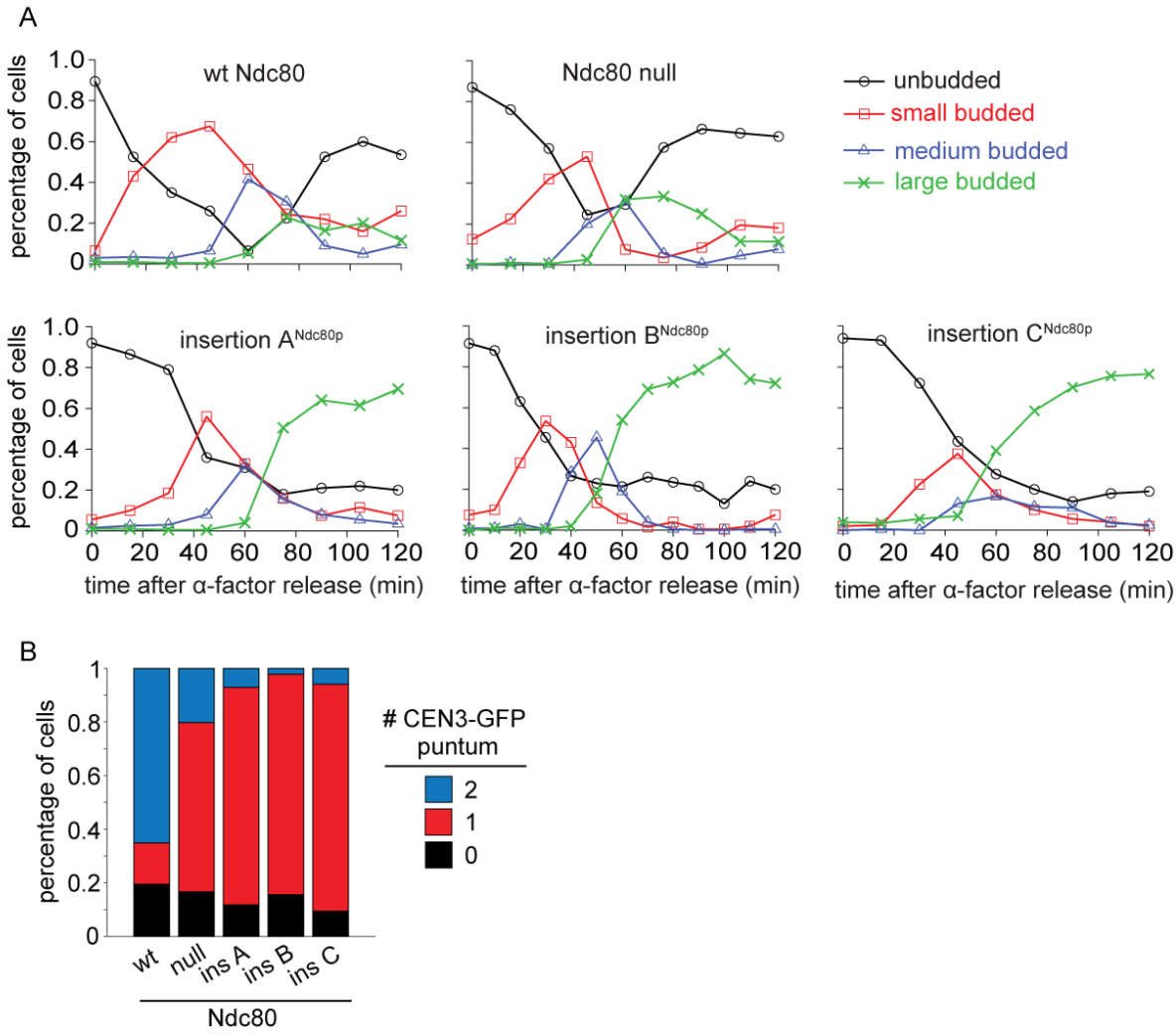

Supplementary Figure 7
Lethal mutation in region A^{Ndc80p}, B^{Ndc80p}, or C^{Ndc80p} causes mitotic arrest
(A) Budding index analyses of Ndc80-AID degron experiments. Ndc80-AID cells carrying an additional copy of *NDC80* wild type, no *NDC80* (null), lethal mutation in region A^{Ndc80p}, B^{Ndc80p}, or C^{Ndc80p} were fixed at various time points after release from α-factor arrest (time 0). (B) Stacked bar graphs showing the proportion of cells with zero, one, or two CEN3-GFP spots for the various cell types.

Table

Table 1. Details of the interaction between Dam1 and Ndc80 complexes

Interaction	protein region	amino acids	Phosphorylated residues	Five amino acid insertion mutation position
A	A^{Dam1p}	241 – 330	S257, S265, S292	n/a
	A^{Ndc80p}	262 – 322	n/a	314
B	B^{Ask1p}	133 – 225	S200	n/a
	B^{Ndc80p}	350 – 448	n/a	383
C	C^{Spc34p}	118 – 274	T199	n/a
	C^{Ndc80p}	532 – 630	n/a	563

Bibliography

Asbury, C. L., Gestaut, D. R., Powers, A. F., Franck, A. D., & Davis, T. N. (2006). The Dam1 kinetochore complex harnesses microtubule dynamics to produce force and movement. *Proceedings of the National Academy of Sciences of the United States of America*, *103*(26), 9873–9878. doi:10.1073/pnas.0602249103

Bharadwaj, R., Qi, W., & Yu, H. (2004). Identification of Two Novel Components of the Human NDC80 Kinetochore Complex. *Journal of Biological Chemistry*, *279*(13), 13076–13085. doi:10.1074/jbc.M310224200

Biggins, S., Severin, F. F., Bhalla, N., Sassoon, I., Hyman, A. a., & Murray, A. W. (1999). The conserved protein kinase Ipl1 regulates microtubule binding to kinetochores in budding yeast. *Genes and Development*, *13*, 532–544. doi:10.1101/gad.13.5.532

Chambers, M. C., Maclean, B., Burke, R., Amodei, D., Ruderman, D. L., Neumann, S., … Mallick, P. (2012). A cross-platform toolkit for mass spectrometry and proteomics. *Nature Biotechnology*, *30*(10), 918–920. doi:10.1038/nbt.2377

Cheeseman, I. M., Anderson, S., Jwa, M., Green, E. M., Kang, J. S., Yates, J. R., … Barnes, G. (2002). Phospho-regulation of kinetochore-microtubule attachments by the Aurora kinase Ipl1p. *Cell*, *111*(2), 163–172. doi:10.1016/S0092-8674(02)00973-X

Cheeseman, I. M., Enquist-Newman, M., Müller-Reichert, T., Drubin, D. G., & Barnes, G. (2001). Mitotic spindle integrity and kinetochore function linked by the Duo1p/Dam1p complex. *Journal of Cell Biology*, *152*(1), 197–212. doi:10.1083/jcb.152.1.197

Davis, T. N. (1992). Mutational analysis of calmodulin in Saccharomyces cerevisiae. *Cell Calcium*, *13*(6-7), 435–444. doi:10.1016/0143-4160(92)90056-X

Dou, Z., Liu, X., Wang, W., Zhu, T., Wang, X., Xu, L., … Yao, X. (2015). Dynamic localization of Mps1 kinase to kinetochores is essential for accurate spindle microtubule attachment. *Proceedings of the National Academy of Sciences*, *112*(33), E4546–E4555. doi:10.1073/pnas.1508791112

Eng, J. K., Jahan, T. A., & Hoopmann, M. R. (2013). Comet: An open-source MS/MS sequence database search tool. *Proteomics*, *13*(1), 22–24. doi:10.1002/pmic.201200439

Gestaut, D. R., Cooper, J., Asbury, C. L., Davis, T. N., & Wordeman, L. (2010). Reconstitution and Functional Analysis of Kinetochore Subcomplexes. *Methods in Cell Biology*, *95*, 641–656. doi:10.1016/S0091-679X(10)95032-2

Gestaut, D. R., Graczyk, B., Cooper, J., Widlund, P. O., Zelter, A., Wordeman, L., … Davis, T. N. (2008). Phosphoregulation and depolymerization-driven movement of the Dam1 complex do not require ring formation. *Nature Cell Biology*, *10*(4), 407–414. doi:10.1038/ncb1702

Hauf, S., Cole, R. W., LaTerra, S., Zimmer, C., Schnapp, G., Walter, R., … Peters, J. M. (2003). The small molecule Hesperadin reveals a role for Aurora B in correcting kinetochore-microtubule attachment and in maintaining the spindle assembly checkpoint. *Journal of Cell Biology*, *161*(2), 281–294. doi:10.1083/jcb.200208092

Hiruma, Y., Sacristan, C., Pachis, S. T., Adamopoulos, A., Kuijt, T., Ubbink, M., … Kops, G. J. P. L. (2015). CELL DIVISION CYCLE. Competition between MPS1 and microtubules at kinetochores regulates spindle checkpoint signaling. *Science (New York, N.Y.)*, *348*(6240), 1264–7. doi:10.1126/science.aaa4055

Hoopmann, M. R., Zelter, A., Johnson, R. S., Riffle, M., Maccoss, M. J., Davis, T. N., & Moritz, R. L. (2015). Kojak: Efficient analysis of chemically cross-linked protein complexes.

Journal of Proteome Research, *14*(5), 2190–2198. doi:10.1021/pr501321h
Ji, Z., Gao, H., & Yu, H. (2015). Kinetochore attachment sensed by competitive Mps1 and microtubule binding to Ndc80C. *Science*, *348*(6240), 1260–1264. doi:10.1126/science.aaa4029
Joglekar, A. P., Bloom, K., & Salmon, E. D. (2009). In Vivo Protein Architecture of the Eukaryotic Kinetochore with Nanometer Scale Accuracy. *Current Biology*, *19*(8), 694–699. doi:10.1016/j.cub.2009.02.056
Joglekar, A. P., Bouck, D. C., Molk, J. N., Bloom, K. S., & Salmon, E. D. (2006). Molecular architecture of a kinetochore-microtubule attachment site. *Nature Cell Biology*, *8*(6), 581–585. doi:10.1038/ncb1414
Kalantzaki, M., Kitamura, E., Zhang, T., Mino, A., Novák, B., & Tanaka, T. U. (2015). Kinetochore–microtubule error correction is driven by differentially regulated interaction modes. *Nature Cell Biology*, *17*(4), 421–433. doi:10.1038/ncb3128
Käll, L., Canterbury, J. D., Weston, J., Noble, W. S., & MacCoss, M. J. (2007). Semi-supervised learning for peptide identification from shotgun proteomics datasets. *Nature Methods*, *4*(11), 923–925. doi:10.1038/nmeth1113
Kudalkar, E. M., Scarborough, E. A., Umbreit, N. T., Zelter, A., Gestaut, D. R., Riffle, M., … Davis, T. N. (2015). Regulation of outer kinetochore Ndc80 complex-based microtubule attachments by the central kinetochore Mis12/MIND complex. *Proceedings of the National Academy of Sciences of the United States of America*, *112*(41), E5583–9. doi:10.1073/pnas.1513882112
Lampert, F., Hornung, P., & Westermann, S. (2010). The Dam1 complex confers microtubule plus end-tracking activity to the Ndc80 kinetochore complex. *Journal of Cell Biology*, *189*(4), 641–649. doi:10.1083/jcb.200912021
Lampert, F., Mieck, C., Alushin, G. M., Nogales, E., & Westermann, S. (2013). Molecular requirements for the formation of a kinetochore-microtubule interface by Dam1 and Ndc80 complexes. *Journal of Cell Biology*, *200*(1), 21–30. doi:10.1083/jcb.201210091
Lawrimore, J., Bloom, K. S., & Salmon, E. D. (2011). Point centromeres contain more than a single centromere-specific Cse4 (CENP-A) nucleosome. *Journal of Cell Biology*, *195*(4), 573–582. doi:10.1083/jcb.201106036
Lupas, A. N., & Gruber, M. (2005). The structure of alpha-helical coiled coils. *Advances in Protein Chemistry*, *70*, 37–78. doi:10.1016/S0065-3233(05)70003-6
Maure, J. F., Komoto, S., Oku, Y., Mino, A., Pasqualato, S., Natsume, K., … Tanaka, T. U. (2011). The Ndc80 loop region facilitates formation of kinetochore attachment to the dynamic microtubule plus end. *Current Biology*, *21*(3), 207–213. doi:10.1016/j.cub.2010.12.050
Miller, M. P., Asbury, C. L., & Biggins, S. (2016). A TOG Protein Confers Tension Sensitivity to Kinetochore-Microtubule Attachments. *Cell*, *165*(6), 1–12. doi:10.1016/j.cell.2016.04.030
Miranda, J. J. L., De Wulf, P., Sorger, P. K., & Harrison, S. C. (2005). The yeast DASH complex forms closed rings on microtubules. *Nature Structural & Molecular Biology*, *12*(2), 138–143. doi:10.1038/nsmb896
Muller, E. G. (1996). A glutathione reductase mutant of yeast accumulates high levels of oxidized glutathione and requires thioredoxin for growth. *Molecular Biology of the Cell*, *7*(11), 1805–1813. Retrieved from http://www.pubmedcentral.nih.gov/articlerender.fcgi?artid=276027{&}tool=pmcentrez{&}

rendertype=abstract
Muller, E. G. D., Snydsman, B. E., Novik, I., Hailey, D. W., Gestaut, D. R., Niemann, C. A., … Davis, T. N. (2005). The organization of the core proteins of the yeast spindle pole body. *Molecular Biology of the Cell*, *16*(7), 3341–52. doi:10.1091/mbc.E05-03-0214
Nishimura, K., Fukagawa, T., Takisawa, H., Kakimoto, T., & Kanemaki, M. (2009). An auxin-based degron system for the rapid depletion of proteins in nonplant cells. *Nature Methods*, *6*(12), 917–922. doi:10.1038/nmeth.1401
Pinsky, B. a, Kung, C., Shokat, K. M., & Biggins, S. (2006). The Ipl1-Aurora protein kinase activates the spindle checkpoint by creating unattached kinetochores. *Nature Cell Biology*, *8*(1), 78–83. doi:10.1038/ncb1341
Powers, A. F., Franck, A. D., Gestaut, D. R., Cooper, J., Gracyzk, B., Wei, R. R., … Asbury, C. L. (2009). The Ndc80 Kinetochore Complex Forms Load-Bearing Attachments to Dynamic Microtubule Tips via Biased Diffusion. *Cell*, *136*(5), 865–875. doi:10.1016/j.cell.2008.12.045
Ramey, V. H., Wong, a., Fang, J., Howes, S., Barnes, G., & Nogales, E. (2011). Subunit organization in the Dam1 kinetochore complex and its ring around microtubules. *Molecular Biology of the Cell*, *22*(22), 4335–4342. doi:10.1091/mbc.E11-07-0659
Sarangapani, K. K., & Asbury, C. L. (2014). Catch and release: How do kinetochores hook the right microtubules during mitosis? *Trends in Genetics*, *30*(4), 150–159. doi:10.1016/j.tig.2014.02.004
Schmidt, J. C., Arthanari, H., Boeszoermenyi, A., Dashkevich, N. M., Wilson-Kubalek, E. M., Monnier, N., … Cheeseman, I. M. (2012). The Kinetochore-Bound Ska1 Complex Tracks Depolymerizing Microtubules and Binds to Curved Protofilaments. *Developmental Cell*, *23*(5), 968–980. doi:10.1016/j.devcel.2012.09.012
Tanaka, T. U., Rachidi, N., Janke, C., Pereira, G., Galova, M., Schiebel, E., … Nasmyth, K. (2002). Evidence that the Ipl1-Sli15 (Aurora Kinase-INCENP) complex promotes chromosome bi-orientation by altering kinetochore-spindle pole connections. *Cell*, *108*(3), 317–329. doi:10.1016/S0092-8674(02)00633-5
Tien, J. F., Fong, K. K., Umbreit, N. T., Payen, C., Zelter, A., Asbury, C. L., … Davis, T. N. (2013). Coupling unbiased mutagenesis to high-throughput DNA sequencing uncovers functional domains in the Ndc80 kinetochore protein of Saccharomyces cerevisiae. *Genetics*, *195*(1), 159–170. doi:10.1534/genetics.113.152728
Tien, J. F., Umbreit, N. T., Gestaut, D. R., Franck, A. D., Cooper, J., Wordeman, L., … Davis, T. N. (2010). Cooperation of the Dam1 and Ndc80 kinetochore complexes enhances microtubule coupling and is regulated by aurora B. *Journal of Cell Biology*, *189*(4), 713–723. doi:10.1083/jcb.200910142
Tien, J. F., Umbreit, N. T., Zelter, A., Riffle, M., Hoopmann, M. R., Johnson, R. S., … Davis, T. N. (2014). Kinetochore Biorientation in Saccharomyces cerevisiae Requires a Tightly Folded Conformation of the Ndc80 Complex. *Genetics*, *198*(December), 1483–1493. doi:10.1534/genetics.114.167775
Umbreit, N. T., Miller, M. P., Tien, J. F., Ortolá, J. C., Gui, L., Lee, K. K., … Davis, T. N. (2014). Kinetochores require oligomerization of Dam1 complex to maintain microtubule attachments against tension and promote biorientation. *Nature Communications*, *5*, 4951. doi:10.1038/ncomms5951
Wargacki, M. M., Tay, J. C., Muller, E. G., Asbury, C. L., & Davis, T. N. (2010). Kip3, the yeast kinesin-8, is required for clustering of kinetochores at metaphase. *Cell Cycle*, *9*(13), 2581–

2588. doi:10.4161/cc.9.13.12076
Wei, R. R., Sorger, P. K., & Harrison, S. C. (2005). Molecular organization of the Ndc80 complex, an essential kinetochore component. *Proc Natl Acad Sci U S A*, *102*(15), 5363–7. doi:10.1073/pnas.0501168102
Welburn, J. P. I., Grishchuk, E. L., Backer, C. B., Wilson-Kubalek, E. M., Yates, J. R., & Cheeseman, I. M. (2009). The Human Kinetochore Ska1 Complex Facilitates Microtubule Depolymerization-Coupled Motility. *Developmental Cell*, *16*(3), 374–385. doi:10.1016/j.devcel.2009.01.011
Westermann, S., Avila-Sakar, A., Wang, H.-W., Niederstrasser, H., Wong, J., Drubin, D. G., … Barnes, G. (2005). Formation of a dynamic kinetochore-microtubule interface through assembly of the Dam1 ring complex. *Molecular Cell*, *17*(2), 277–290. doi:10.1016/j.molcel.2004.12.019
Widlund, P. O., & Davis, T. N. (2005). A high-efficiency method to replace essential genes with mutant alleles in yeast. *Yeast*, *22*(10), 769–774. doi:10.1002/yea.1244
Zelter, A., Bonomi, M., Kim, J. ook, Umbreit, N. T., Hoopmann, M. R., Johnson, R., … Davis, T. N. (2015). The molecular architecture of the Dam1 kinetochore complex is defined by cross-linking based structural modelling. *Nature Communications*, *6*, 8673. doi:10.1038/ncomms9673